

Article

# Synthesis and Structure of Unsymmetrical Anthracenyl-Isoxazole Antitumor Agents Via the Diastereoselective Bromination of 3-(9'-Anthryl)-Isoxazole Esters

Michael J. Campbell <sup>1,†</sup>, Daniel A. Decato <sup>1</sup>, Chun Li <sup>2</sup>, Matthew J. Weaver <sup>1,‡</sup>  and Nicholas R. Natale <sup>1,\*</sup> 

<sup>1</sup> Medicinal Chemistry Graduate Program, University of Montana, Missoula, MT 59812, USA; mjcampbell@osrxpharmaceuticals.com (M.J.C.); daniel.decato@mso.umt.edu (D.A.D.); weaver@silicongases.com (M.J.W.)

<sup>2</sup> Department of Chemistry, Ithaca College, 953 Danby Road, Ithaca, NY 14850, USA; cli6@ithaca.edu

\* Correspondence: nicholas.natale@umontana.edu

† Current address: OSRX Pharmaceuticals, Missoula, MT 59801, USA.

‡ Current address: Advanced Material Solutions, 2920 S Garfield Street, Missoula, MT 59801, USA.

**Abstract:** In pursuit of unsymmetrical precursors for the novel series of anthracenyl-isoxazole amide (AIM) antitumor agents, a series of substituted anthracenes were subjected to bromination and re-aromatization in our study, during which we solved four single crystal X-ray diffraction (Sc-xrd) structures which we report herein. The C-9 nitrile oxide, after its reaction with bromine, was isolated, but when subjected to re-aromatization, it returned to the starting 10-bromo nitrile oxide **1**, which did provide an accurate crystal structure, with  $R = 0.018$ . The 10-halogenated 3-(9'-anthryl)-isoxazole esters were subjected to bromination and re-aromatization. Surprisingly, the yields obtained in the presence of the isoxazole were reasonably good (62–68% isolated yields), and the major diastereomers allowed for the characterization using Sc-xrd. The penta bromo product **2** showed a *trans, trans, cis* relationship for the four bromines on the A-ring of the anthracene, and we observed that for the unit cell, the atropisomers displayed a 1:1 ratio at the chiral axis between the isoxazole and anthracene rings. Similarly, the 10-chloro **3** indicated a ratio of 1:1 at the chiral axis in the crystal structure. A base-induced re-aromatization afforded 3,10-dihalogenated analogues selectively in very good yields ( $X = \text{Cl}$ , 89%;  $X = \text{Br}$  92%), of which the dibromo **4** was characterized using Sc-xrd. The improved yields of the unique diastereomeric bromination products suggested the consideration of a novel electrophilic aromatic substitution mechanism driven by the stereo-electronic environment, imposed by the isoxazole ester substituent. The promise of the application of this chemistry in the future development of AIM antitumor agents is suggested.

**Keywords:** anthracene; atropisomerism; axial chirality; bromination; isoxazole



**Citation:** Campbell, M.J.; Decato, D.A.; Li, C.; Weaver, M.J.; Natale, N.R. Synthesis and Structure of Unsymmetrical Anthracenyl-Isoxazole Antitumor Agents Via the Diastereoselective Bromination of 3-(9'-Anthryl)-Isoxazole Esters. *Crystals* **2024**, *14*, 256. <https://doi.org/10.3390/cryst14030256>

Academic Editors: Blaine Mooers and Jolanta Prywer

Received: 5 February 2024

Revised: 21 February 2024

Accepted: 25 February 2024

Published: 5 March 2024



**Copyright:** © 2024 by the authors. Licensee MDPI, Basel, Switzerland. This article is an open access article distributed under the terms and conditions of the Creative Commons Attribution (CC BY) license (<https://creativecommons.org/licenses/by/4.0/>).

## 1. Introduction

The DNA secondary structure known as the G-quadruplex (G4s) consists of therapeutically interesting folding motifs found in single-stranded DNA [1–3]. The G4s are formed in guanine-rich regions of DNA that, when folded, form multiple planar decks known as G-quartets that are stabilized by Hoogsteen base pairing between four guanines. These G-decks are stabilized by cations (usually  $\text{K}^+$ ) that occupy the cavity left in the middle of the stacking G-decks. These guanine-rich G4-forming sequences of DNA or RNA are found in telomeres and oncogene promoter regions and are thought to have a regulatory role in transcription. The stabilization of these G4 structural motifs has been shown to suppress gene expression, and over the past two decades, they have become a target of interest in the field of antitumor small molecules. These small molecules have been shown to bind G-quadruplex DNA through favorable interactions with one or more of the following structural features: stacking with the G-decks, binding in the minor groove, interactions with the extrahelical bases, and electrostatic interactions with the sugar–phosphate backbone [1–3].

Our working hypothesis for the antitumor activity of a series of compounds developed in our laboratory, termed aryl isoxazole amides (AIMs), has evolved as our studies have progressed. Our original hypothesis was that aryl isoxazole lexitropsin conjugates could plausibly bind the minor groove of B-DNA [4,5]. As our experimental studies of the process continued, the interaction with DNA G-quadruplex structures, via a combination of stacking with the G-decks, and interactions with the sugar–phosphate backbone and extrahelical bases, was supported by G4 DNA melting experiments, 2D NMR titration studies, computational docking, and molecular dynamics experiments [6]. We have previously reported the quadruplex-binding small molecules known as AIMs have displayed tumor growth inhibition in the micro- to sub-micromolar range against breast cancer, as well as human and rat glioma cell lines [5–7]. Most recently, we expanded our working hypothesis to the ternary complex of G4, with its helicase in combination with the antitumor AIM [7]. In recent generations of AIM small molecules, we have addressed the bioavailability concerns revolving around the lipophilicity of the anthracene moiety [6] and continued to develop the structure–activity relationship and increase the potency [5–7]. However, one main concern raised in the pursuit of G-4 quadruplexes as viable therapeutic targets is the structural similarity and ubiquitous presence of quadruplexes in all cell types that could lead to unwanted polypharmacology [1]. Herein we report the structure of four brominated isoxazole structures pursuant to the improvement of efficacy and selectivity of the aryl isoxazole antitumor agents (Figure 1).

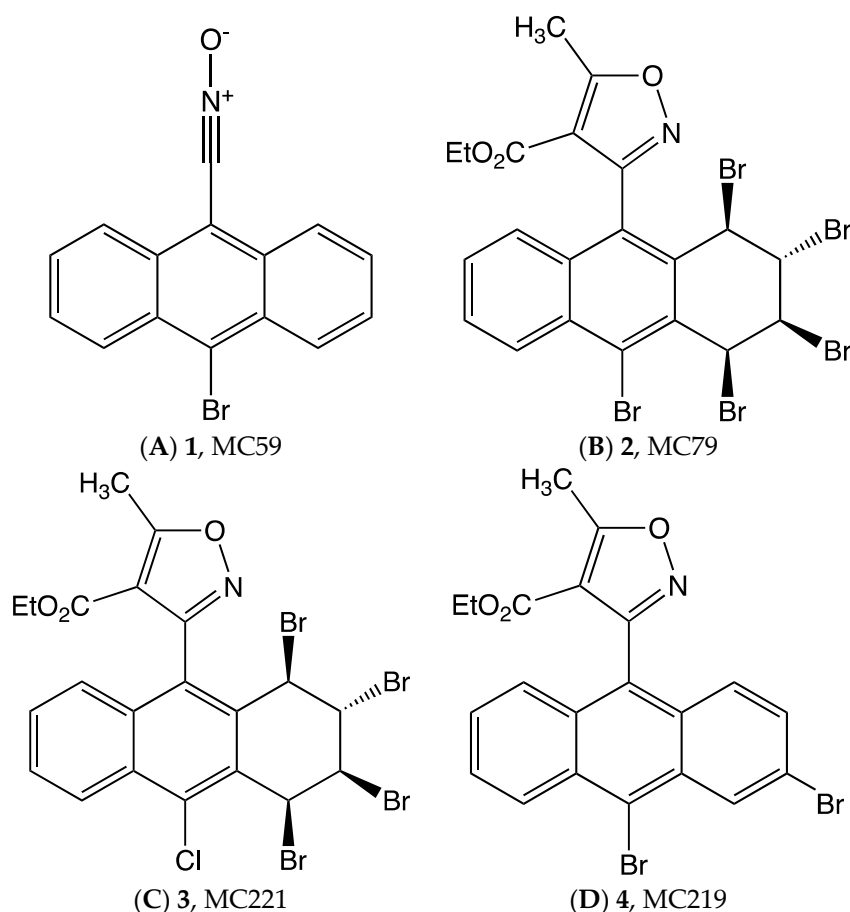
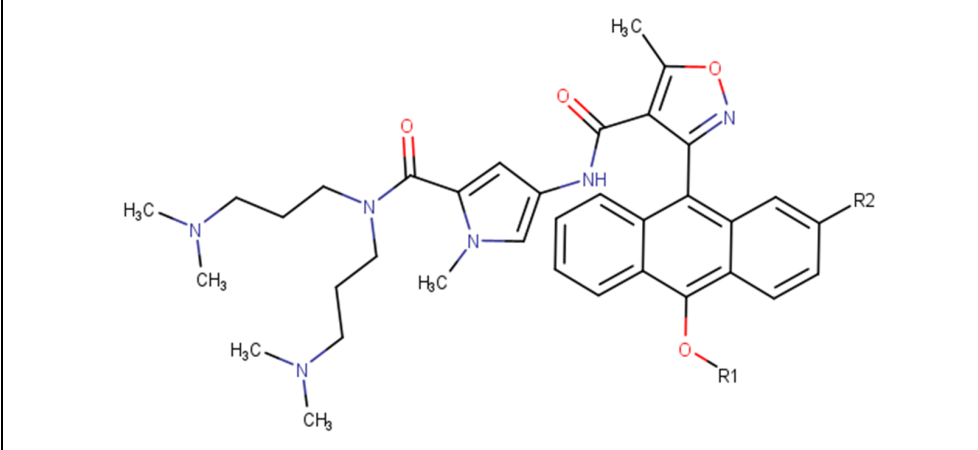


**Figure 1.** New Sc-xrd of 4 brominated anthracenes obtained in the current study. (A). Bromo nitrile oxide, 1, MC-59. (B). Penta bromo isoxazole ester 2, MC-79. (C). Tetra bromo chloro isoxazole ester, 3, MC-221. (D). Dibromo isoxazole ester 4, MC-219.

The inherent chirality of DNA offers a possible path to designing small molecules that address the issue of specificity, as compounds that possess a chiral characteristic

often display differences in their activity and selectivity in biological systems, resulting in eudismic ratios or even the presence or absence of off-site toxicity [8]. The unique three-dimensional conformation brought about by the orthogonal orientation of the isoxazole ring to the anthracene moiety, observed in computational experiments with G4 [9] as well as many AIM precursor crystal structures (Figure 2), provides a potential axis of chirality were the anthracene to be substituted unsymmetrically. Asymmetry about the C(3) aryl-isoxazole axis would impart an atropisomeric characteristic to the compound, and depending on the energetic barrier to rotation, may lock the compound in a conformation, resulting in isolable enantiomers. Early efforts to explore this possibility led to promising results.



IC <sub>50</sub> μM (SD)	R <sub>1</sub>	R <sub>2</sub>	-CDocker Energy (kcal/mole)
7.77 (1.11)	-CH <sub>3</sub>	H	71.943
4.8 (0.80)	-CH <sub>3</sub>	-OCH <sub>3</sub>	P 76.37 M 78.1

**Figure 2.** Cytotoxicity activity against SNB-19 human glioma cells paired with the corresponding predicted docking energies at G-4 coordinates PDB ID 2L7V.

The cytotoxicity studies performed on human glioma cells (SNB-19 cells) using 10-alkoxy-anthracenyl-isoxazole analogues, outlined in Figure 2, provide evidence that the unsymmetrical 2,10-dimethoxy AIM has an improved antitumor activity over the symmetrical 10-methoxy AIM. Additionally, the computational docking experiments, also noted in Figure 2, suggest that there exists a preference for the (M)-atropisomer over the (P)-atropisomer, with the M conformer having a more favorable binding energy as well as assigned interaction for the (M)-2-methoxy substituent, which exhibited an interaction with the dG8 sugar-phosphate backbone (Figure 3A) [7]. Although computational docking is not a direct reflection of nature, these results combine to indicate a promising route to increased activity through the synthesis of unsymmetrical and conformationally locked atropisomers. Although successful as a proof of concept, our original pathway to the unsymmetrical AIM lacked a key intermediate that is synthetically flexible to aid in the diversification of later generations of AIMs. Ideally, the design of an unsymmetrical precursor in the AIM series would include a convenient synthetic handle, such as a halogen, that could be used to easily diversify AIM analogues to explore and expand our understanding of the structure-activity relationship.

A second potential use for unsymmetrically halogenated AIMs was suggested during our consideration of the plausible metabolic fates of the anthracene. One of our planned roles for the isoxazoles was to direct Cyp3A4 metabolism away from potentially toxic metabolites at the anthracene ring, and both prior models in the literature [11] and Smart-Cyp density function computations [12] suggest that hydroxylation at the C-5 alkyl group of the isoxazole is a reasonable route; however, the docking of the alkoxy AIM shown

presents the side of the anthracene directly over the heme of the Cyp [13] (Figure 3B). We decided that we should anticipate this by using the tactic of blocking the position with a halogen, and a bromine could provide either a metabolism blocking effect intrinsically (as in Vandetanib [14]) or serve as a precursor to the strategically positioned fluorine [15,16].

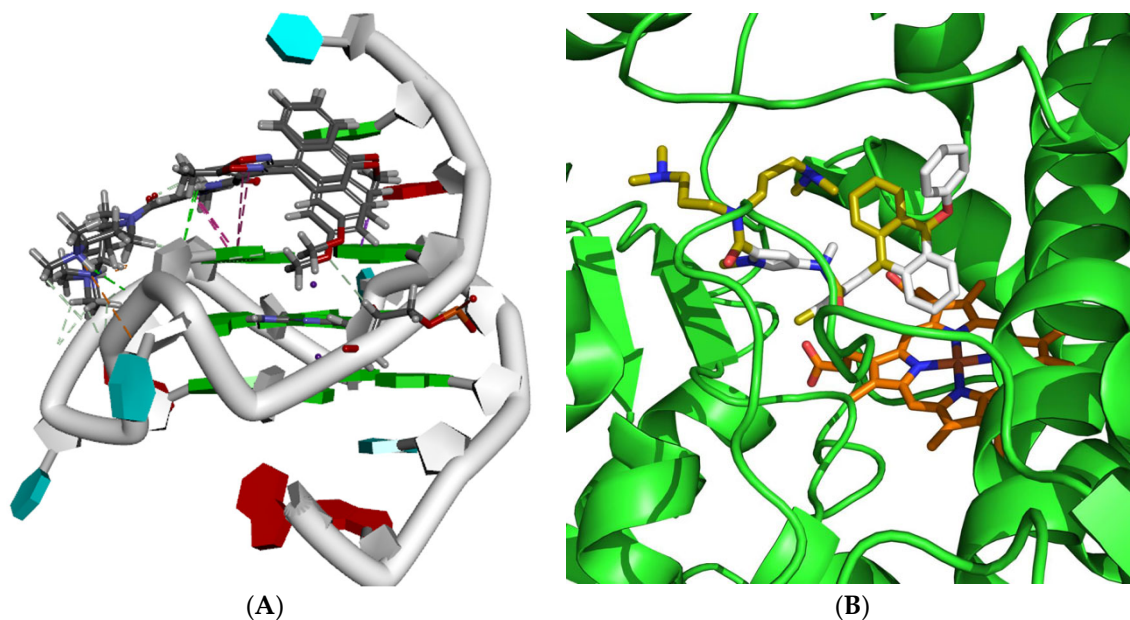


**Figure 3.** (A). Docking of the 2,10-dimethoxy AIM at the putative G4 DNA target (pdb accession number 2L7V [9]) gave a reasonable explanation for its higher efficacy against tumor cell lines. (B). In some docked poses, the anthracene presents protons toward the metabolizing Cyp3A4 heme (pdb accession number 3NXU [10]).

## 2. Materials and Methods

### 2.1. Materials: Chemistry

The isoxazole anthracenes used in this study have been previously described [17], they were prepared using nitrile oxide cycloaddition [18]. The bromination procedures were previously pioneered by the thorough and careful work of the Cakmak group [19,20].

#### 2.1.1. General Procedure for The Bromination Reactions

The crystalline 10-halogenated anthracenyl isoxazole ethyl ester was dissolved in dry dichloromethane, and the solution was stirred at  $-15\text{ }^{\circ}\text{C}$  as excess elemental bromine was diluted in dichloromethane and added to the stirring solution. The reaction mixture was then placed in the freezer and left to react in the dark for 20 days.

The reaction was then removed from the freezer and the excess bromine in the reaction mixture was deactivated using a solution of sodium metabisulfite. The deactivated solution was then transferred to a separatory funnel and was washed with deionized water. The combined organic fractions were then washed with brine, dried over anhydrous sodium sulfate, filtered, and concentrated. The concentrated product was then purified by silica gel chromatography using a mixture of 10:1:1 hexanes:dichloromethane:ethyl acetate.

Ethyl 5-methyl-3-[(1R,2S,3S,4S)-1,2,3,4,10-pentabromo-1,2,3,4,4a,9a-hexahydroanthracen-9-yl]-1,2-oxazole-4-carboxylate, **2** (MC79): Pure crystalline 10-bromo anthracenyl isoxazole ethyl ester (0.5 mmol) was dissolved in dry dichloromethane (7 mL) and cooled to  $-15\text{ }^{\circ}\text{C}$ . To the stirring solution, four equivalents of elemental bromine (2 mmol) diluted with dichloromethane (1 mL) were added. The reaction mixture was moved to the freezer and allowed to react in the absence of light at  $-15\text{ }^{\circ}\text{C}$  for 20 days. The reaction was removed from the freezer after 20 days, the excess bromine was deactivated with sodium metabisulfite, and the organic layer was transferred to a separatory funnel and washed with deionized water. The combined organic fractions were then washed with

brine, dried over anhydrous sodium sulfate, filtered, and concentrated. The concentrated product was then purified by silica gel chromatography using a mixture of 10:1:1 hexanes:dichloromethane:ethyl acetate. The purified compound was crystallized from the column fractions, and the yield was calculated to be 68%.

$^1\text{H}$  NMR (400 MHz,  $\text{CHCl}_3\text{-d}$ )  $\delta$  = 8.40 (d,  $J$  = 8.9 Hz, 1H), 7.68 (t,  $J$  = 7.7 Hz, 1H), 7.51 (t,  $J$  = 7.6 Hz, 1H), 7.39 (d,  $J$  = 8.5 Hz, 1H), 6.09 (d,  $J$  = 2.9 Hz, 1H), 6.07 (d, 4.1 Hz, 1H), 5.22 (dd,  $J$  = 4.1, 11.2, 1H), 4.38 (dd,  $J$  = 2.9, 11.2, 1H), 3.79 (q,  $J$  = 7.2, 2H), 2.91 (s, 3H), 0.50 (t,  $J$  = 7.2, 3H). Mass spectrum: calculated MW: 729.877, observed ( $M + 1$ ): 727.54 (48.95% relative intensity), 729.54 (100), 731.54 (98.4), 733.54 (48.2).

#### 2.1.2. Ethyl 5-Methyl-3-[(1*r*,2*s*,3*s*,4*s*)-1,2,3,4-Tetrabromo-10-Chloro-1,2,3,4,4a,9a-Hexahydroanthracen-9-yl]-1,2-Oxazole-4-Carboxylate, 3 (MC221)

Pure crystalline 10-chloro anthracenyl isoxazole ethyl ester (4.46 mmol) was dissolved in dry dichloromethane (30 mL) and cooled to  $-15$  °C. To the stirring solution, four equivalents of elemental bromine (17.8 mmol) diluted with dichloromethane (10 mL) were added. The reaction mixture was moved to the freezer and allowed to react in the absence of light at  $-15$  °C for 20 days. The reaction was removed from the freezer after 20 days, the excess bromine was deactivated with sodium metabisulfite, and the organic layer was transferred to a separatory funnel and washed with deionized water. The combined organic fractions were then washed with brine, dried over anhydrous sodium sulfate, filtered, and concentrated. The concentrated product was then purified by silica gel chromatography using a mixture of 10:1:1 hexanes:dichloromethane:ethyl acetate. The purified compound was crystallized from the column fractions, and the yield was calculated to be 63%.

$^1\text{H}$  NMR (400 MHz,  $\text{CHCl}_3\text{-d}$ )  $\delta$  = 8.39 (d,  $J$  = 8.1 Hz, 1H), 7.69 (t,  $J$  = 7.5 Hz, 1H), 7.53 (t,  $J$  = 7.5 Hz, 1H), 7.42 (d,  $J$  = 8.2 Hz, 1H), 6.08 (d,  $J$  = 3.0 Hz, 1H), 6.06 (d, 4.2 Hz, 1H), 5.22 (dd  $J$  = 4.1, 11.3, 1H), 4.38 (dd,  $J$  = 3.0, 11.3, 1H), 3.79 (q,  $J$  = 7.1, 2H), 2.89 (s, 3H), 0.50 (t,  $J$  = 7.1, 3H).

#### 2.1.3. General Procedure for The Re-Aromatization Reactions

The crystalline 10-halo 1,2,3,4-Br anthracenyl isoxazole ethyl ester was dissolved in pyridine and stirred for 24 h. The resulting reaction mixture was then deactivated with sodium metabisulfite, extracted with diethyl ether, and run through a silica plug before being dried over anhydrous sodium sulfate and purified by silica gel chromatography using a 10:1:1 mixture of hexanes:dichloromethane:ethyl acetate.

#### 2.1.4. Ethyl 3-(3,10-dibromoanthracen-9-yl)-5-methyl-1,2-oxazole-4-carboxylate, 4, (MC219)

The crystalline 10,1,2,3,4-Br anthracenyl isoxazole ethyl ester (0.7027 mmol) was dissolved in pyridine (9.5 mL) and stirred for 24 h. The resulting reaction mixture was then deactivated with sodium metabisulfite, extracted with diethyl ether, and run through a silica plug before being dried over anhydrous sodium sulfate and purified by silica gel chromatography using a 10:1:1 mixture of hexanes:dichloromethane:ethyl acetate. The purified compound was crystallized from the column fractions, and the yield was calculated to be 92%.

$^1\text{H}$  NMR (400 MHz,  $\text{CHCl}_3\text{-d}$ )  $\delta$  = 8.81 (s, 1H), 8.59 (d,  $J$  = 8.4 Hz, 1H), 7.65–7.61 (m, 2H), 7.51–7.46 (m, 3H), 3.74 (q,  $J$  = 6.8, 2H), 2.93 (s, 3H), 0.45 (t,  $J$  = 7.1, 3H). Mass Spectrum for  $\text{C}_{21}\text{H}_{15}\text{Br}_2\text{NO}_3$  calculated MW 489.16, observed 488 (50% relative intensity); 490 (100); 492 (50).

#### 2.1.5. Ethyl 3-(3-bromo-10-chloroanthracen-9-yl)-5-methyl-1,2-oxazole-4-carboxylate

The crystalline 10-halo 1,2,3,4-Br anthracenyl isoxazole ethyl ester was dissolved in pyridine and stirred for 24 h. The resulting reaction mixture was then deactivated with sodium metabisulfite, extracted with dichloromethane, and run through a silica plug before being dried over anhydrous sodium sulfate and purified by silica gel chromatography using a 10:1:1 mixture of hexanes:dichloromethane:ethyl acetate. The isolated and purified

yield was calculated to be 89%. The  $^1\text{H}$  NMR (400 MHz,  $\text{CHCl}_3\text{-d}$ ) of this product was very similar to **4** above, but it was easily distinguished by its respective isotope signatures in the mass spectrum.

## 2.2. Methods: Diffraction

Single crystals from compounds **1** and **2** with suitable sizes and diffracting qualities were mounted on MiTeGen loops (MiTeGen, LLC, Ithaca, NY, USA). The diffraction data were collected at 100 K on a Bruker D8 Discover diffractometer (Bruker AXS Inc., Madison, WI, USA) equipped with a Smart Breeze CCD detector using  $\text{MoK}\alpha$  radiation, with  $\lambda = 0.71073 \text{ \AA}$ . The collected data were processed with APEX2 programs [21] and were corrected for absorption using SADABS, version 2016/2 [22]. The structures were solved with intrinsic phasing methods using SHELXT [23] and refined by the full-matrix least-squares method of  $F^2$  using SHELXL, version 2018/1 [24], as implemented in the OLEX2, version Olex2-1.5 [25].

X-ray diffraction data for **3**, MC221 and **4**, MC219 were collected at 100 K on a Bruker D8 Venture using  $\text{MoK}\alpha$ -radiation ( $\lambda = 0.71073 \text{ \AA}$ ). The data have been corrected for absorption using the SADABS [26] area detector absorption correction program. Using Olex2 [25], the structure was solved with the SHELXT structure solution program, version 2018/2, using direct methods and refined with the SHELXL refinement package, version 2018/3, using least squares minimization. All non-hydrogen atoms were refined with anisotropic thermal parameters. Hydrogen atoms were found in the residual density maps and were eventually placed in calculated positions using a ridged group model with isotropic thermal parameters. Calculations and the refinement of structures were carried out using APEX, version APEX3 [27], SHELXTL [28], and Olex, version Olex2-1.3 [25] software.

Complete crystallographic data for the structure of compounds in this paper have been deposited in the CIF format with the joint CCDC/FIZ Karlsruhe deposition service. The deposition numbers are as follows: compound **1** (MC59): 2324156, compound **2** (MC79): 2324157; compound **3** (MC221, mt-nn2: 2088830; and compound **4** (MC219, mt-nn3: 2088831). These data, can be obtained free of charge via <http://www.ccdc.cam.ac.uk/conts/retrieving.html> (accessed on 26 February 2024).

## 3. Results and Discussion

Aryl nitrile oxides have previously been reported to be isolable [17,29–31], and examples exist of their crystallography [32,33]. We did find it astounding that an anthracene nitrile oxide could be brominated and the pentabromo intermediate could be isolated and purified (Figure 4), although the yield was relatively low (~20%). The stereochemistry of the A-ring tetra bromination was assigned using the Karplus equation through an analogy to the work of Cakmak as *trans*, *cis*, *trans*. On attempting re-aromatization, we found to our dismay that all four of the bromides in the A-ring were lost; thus, the synthetic utility towards our original goal was nil. However, the bromo nitrile oxide **1** we isolated was nicely crystalline, and we obtained the most accurate structure we have ever managed to observe (Figure 5,  $R_1 = 0.018$ , Table 1). Perhaps unsurprisingly, the unit cell is a  $\pi$ -stacked array (Figure 6), but one unique observation is the presence of a prominent intermolecular halogen bond (Figure 7). Both the unit cell and strength of the intramolecular halogen bond can be attributed to the inductive effect of the nitrile oxide [34]. The following can be found in the Supplementary Materials related to the bromo nitrile oxide **1**: Figure S1. Proton NMR of tetrabromo nitrile oxide intermediate **6**, larger versions of Figures 5–7 (Figures S2–S4 respectively), Table S1 Fractional atomic coordinates and isotropic or equivalent isotropic displacement parameters ( $\text{\AA}^2$ ), Table S2. Atomic displacement parameters ( $\text{\AA}^2$ ), and Table S3. Geometric parameters ( $\text{\AA}$ ,  $^\circ$ ).

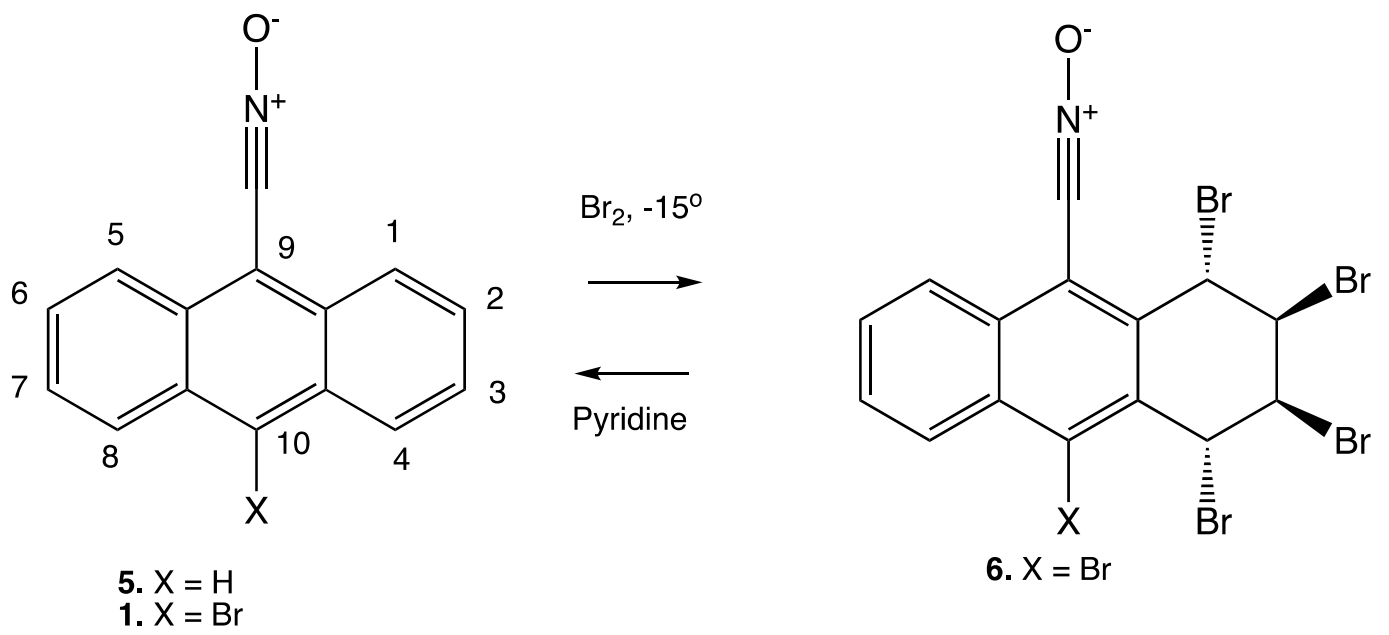


Figure 4. Synthesis of bromo nitrile oxide 1, MC59.

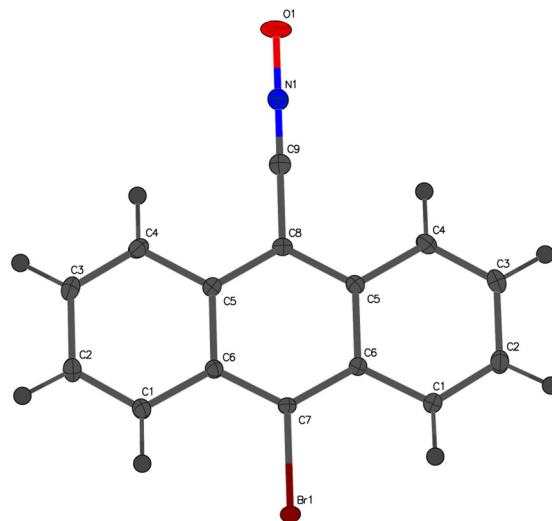


Figure 5. Structure of bromo nitrile oxide 1 (MC59).

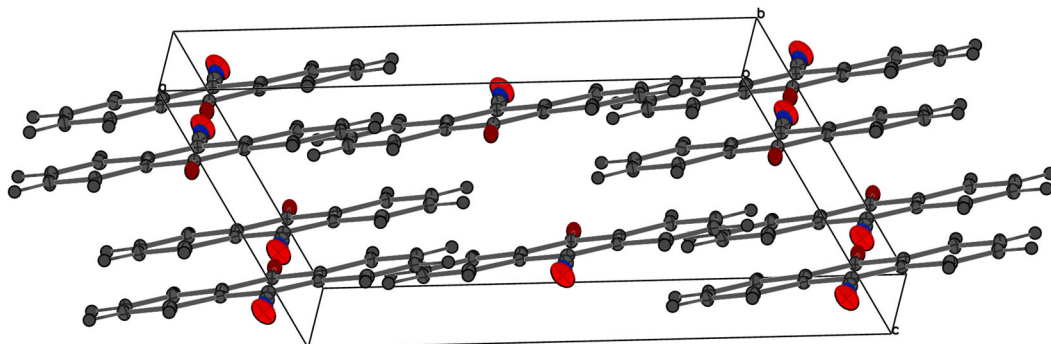
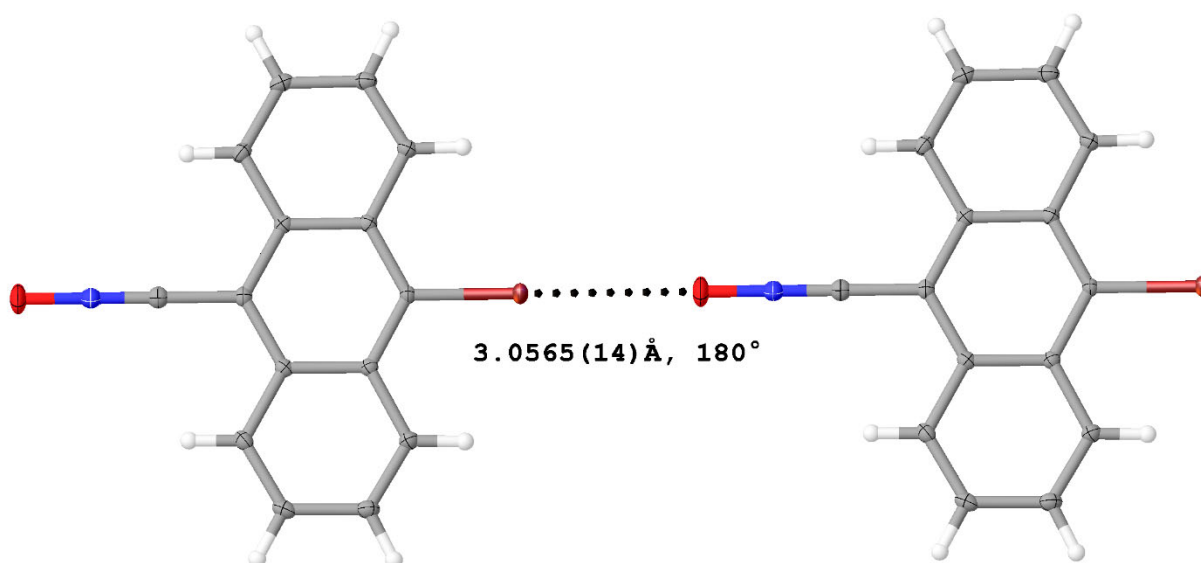


Figure 6. Unit cell for the bromo nitrile oxide 1 (MC59).

**Table 1.** Crystal data, data collection, and structure refinement details for the compounds 1–4 studied using Sc-xrd.

Compound	1, Br-Nitrile Oxide (MC59)	2, Penta-Br (MC79)	3, TetraBr,10-Cl (MC221)	4, Di-Br (MC219)
<i>Crystal Data</i>				
Empirical formula	C <sub>15</sub> H <sub>8</sub> BrNO	C <sub>21</sub> H <sub>16</sub> Br <sub>5</sub> NO <sub>3</sub>	C <sub>21</sub> H <sub>16</sub> Br <sub>4</sub> ClNO <sub>3</sub>	C <sub>21</sub> H <sub>15</sub> Br <sub>2</sub> NO <sub>3</sub>
Formula weight	298.13	729.90	685.44	489.16
Space group	<i>I</i> 12/ <i>c</i> 1	<i>P</i> 2 <sub>1</sub> / <i>n</i>	<i>P</i> 2 <sub>1</sub> / <i>c</i>	<i>P</i> -1
<i>a</i> /Å	12.7115 (7)	18.8346 (6)	23.9057 (8)	8.2647 (5)
<i>b</i> /Å	11.5513 (5)	10.1670 (3)	10.1752 (4)	10.6403 (6)
<i>c</i> /Å	7.3873 (3)	48.1071 (16)	18.6641 (7)	11.9185 (7)
$\alpha$ /°			90	114.342 (2)
$\beta$ /°	92.121 (2)	96.431 (2)	95.2636 (14)	99.388 (2)
$\gamma$ /°			90	98.989 (2)
Volume/Å <sup>3</sup>	1083.97 (9)	9154.1 (5)	4520.8 (3)	912.55 (9)
<i>Z</i>	4	16	8	2
<i>D</i> <sub>x</sub> mg/m <sup>3</sup>	1.827	2.118	2.014	1.780
$\mu$ /mm <sup>1</sup>	3.78	8.80	7.264	4.464
F(000)	592	5568	2640.0	484
Crystal appearance	Needle, dark yellow	Prism	Monoclinic	
Crystal size/mm <sup>3</sup>	0.43 × 0.12 × 0.09	0.31 × 0.29 × 0.21	0.2 × 0.1 × 0.05	0.2 × 0.15 × 0.05
<i>Data Collection</i>				
Radiation ( $\lambda$ )	MoK $\alpha$ 0.71073	MoK $\alpha$ ( $\lambda$ = 0.71073)	MoK $\alpha$ ( $\lambda$ = 0.71073)	MoK $\alpha$ ( $\lambda$ = 0.71073)
$\Theta$ /°	2.4–30.5°	2.5–27.2°	5.804–55.164	5.856–55.046
Index ranges	−18 ≤ <i>h</i> ≤ 18 −13 ≤ <i>k</i> ≤ 16 −9 ≤ <i>l</i> ≤ 10	<i>h</i> = −25→23 <i>k</i> = −13→13 <i>l</i> = −64→64	−31 ≤ <i>h</i> ≤ 31 −13 ≤ <i>k</i> ≤ 13 −24 ≤ <i>l</i> ≤ 24	−10 ≤ <i>h</i> ≤ 10 −13 ≤ <i>k</i> ≤ 13 −15 ≤ <i>l</i> ≤ 15
Measured reflections	6567	140,298	207,255	46,594
Independent reflections	1666	22,760	10,423	4198
Reflections with <i>I</i> > 2 $\sigma$ ( <i>I</i> )	1639	14,809		
<i>Refinement</i>				
Parameters	101	1093		
Goodness-of-fit on F <sup>2</sup>	1.14	1.14	1.087	1.073
R[F <sup>2</sup> > 2 $\sigma$ (F <sup>2</sup> )]	0.018	0.070	0.0403	0.03
wR(F <sup>2</sup> )	0.051	0.137	0.0880	
Largest diff. peak/hole/e Å <sup>−3</sup>	0.63/−0.24	2.19/−1.39	2.83/−0.93	2.41/−0.54
<i>Calculated Features</i>				
C(3) aryl-isoxazole dihedral angle (°)	NA	A 110.4 (3) B 105.1 (3) C 65.4 (3) D 67.6 (3)	A 64.10B 67.26	76.18



**Figure 7.** Halogen bond for bromo nitrile oxide **1** (MC59), with a Br...O distance of 3.0565(14) Å and a C–Br...O angle of 180°.

Using methodology adapted from Cakmak [19], we developed a straightforward route to AIM precursors that allows for the incorporation of a diversity point late in the synthetic scheme. By careful bromination of the 10-Br anthracenyl isoxazole ethyl ester at a low temperature in the absence of light, we were able to produce an unsymmetrical 1,2,3,4,10-Br analogue (Figure 8). The major diastereomer was then isolated and purified and was initially characterized and assigned the stereochemistry of the brominated A-ring of the anthracene using  $^1\text{H}$ NMR. With respect to the proximity of the isoxazole group, we then verified the assigned stereochemistry using single-crystal X-ray diffraction (Sc-xrd) as *trans*, *trans*, *cis* (Figure 9). The asymmetric unit of compound **2** is composed of four molecules, with all four molecules in the unit cell possessing the same A-ring diastereomer. There is some disorder observed in the unit cell; however, most of it is centered on the ethyl ester groups as shown in Figure 9B. We observed that for the unit cell, the atropisomers had a 1:1 ratio. Similar to compound **1**, in the closely packed crystal of compound **2**, prominent intermolecular halogen–halogen, halogen heteroatom, and halogen–hydrogen short contacts that are in the range of 3.0 to 3.5 Å are observed. For example, pairs of molecules A and C form a zigzag chain through the intermolecular Br...Br contacts between the alternating Br2 and Br5 in molecules A and C. This chain, running along an *a*-axis, is perpendicular to the 100 plane. Four chains running along the *b*-axis and perpendicular to the 010 plane are formed by Br3A...O1A', Br3B...O1B', Br3C...O1C', and Br3D...O1D' contacts in molecules A, B, C, and D, respectively. These chains are crosslinked by halogen–halogen and halogen–hydrogen short contacts to give an overall layers of sheets that is parallel to the 001 plane. Each sheet is composed of either A/C pairs or B/D pairs of molecules, with each pair composed of the opposite atropisomers, thus making the whole crystal symmetric. The following can be found in the Supplementary Materials for penta bromo ester **2** (MC79): Figure S5. Proton NMR, Figure S6.  $^{13}\text{C}$  NMR, Figure S7. Numbering of unit cell, Table S4. Fractional atomic coordinates and isotropic or equivalent isotropic displacement parameters ( $\text{Å}^2$ ), Table S5. Atomic displacement parameters ( $\text{Å}^2$ ), Table S6. Geometric parameters ( $\text{Å}$ ,  $^\circ$ ), and Table S7. Hydrogen-bond geometry ( $\text{Å}$ ,  $^\circ$ ).

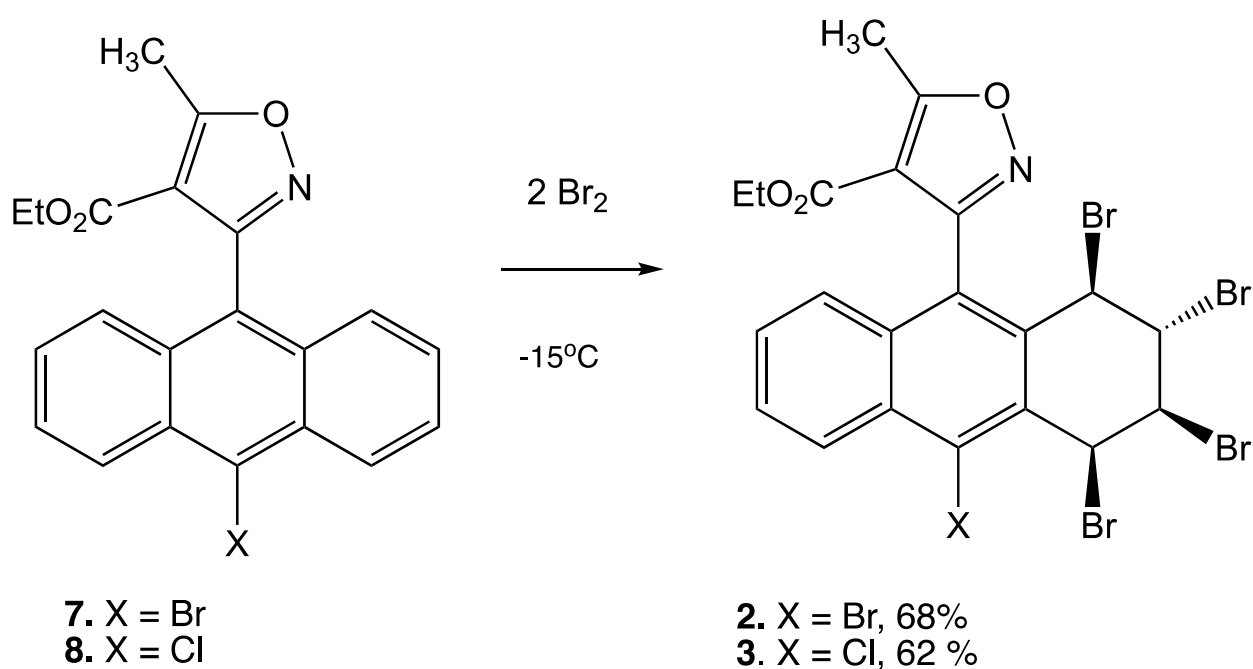


Figure 8. Exhaustive bromination of the A-ring of AIMs where X = Br or Cl.

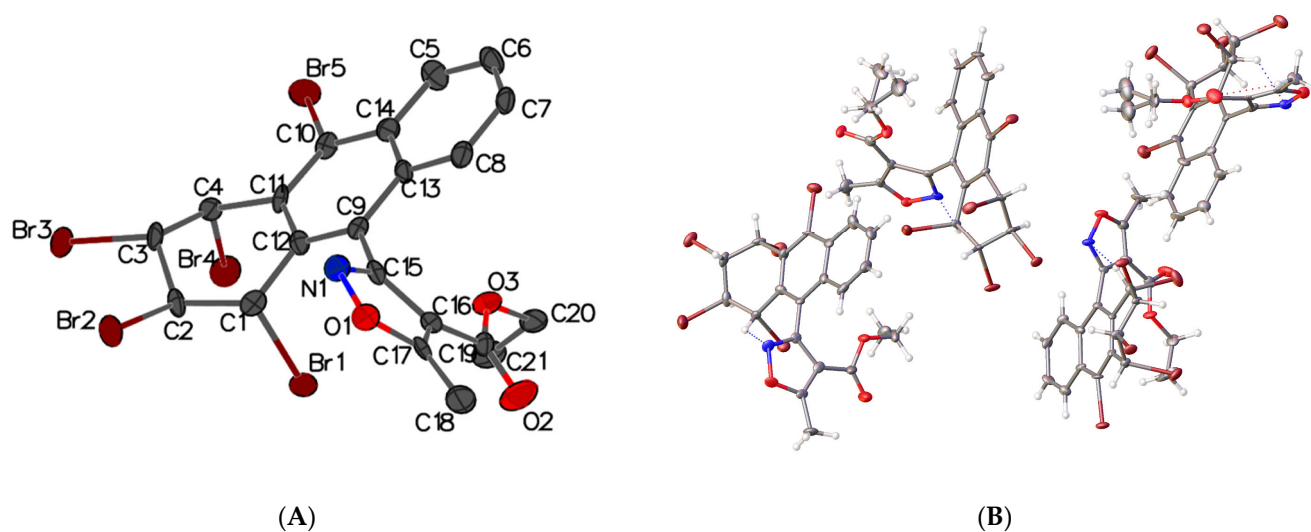
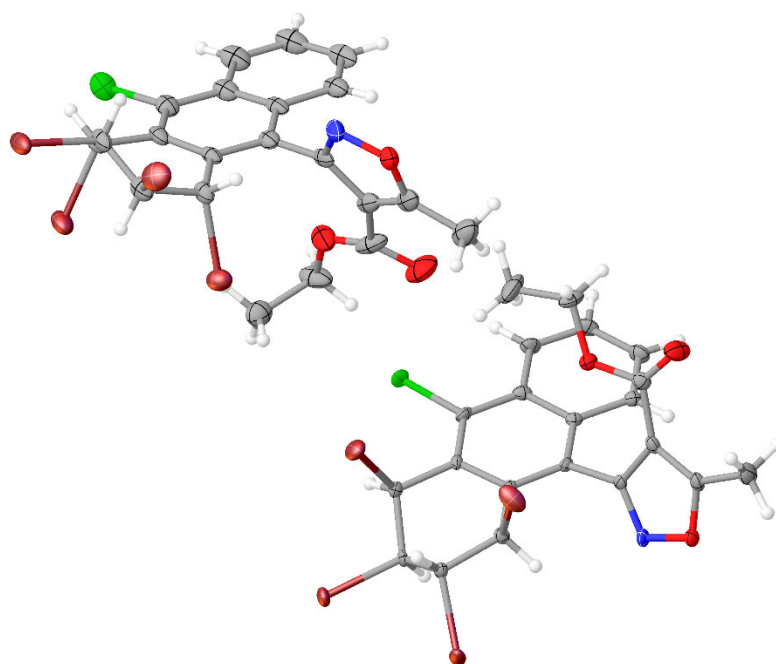


Figure 9. (A). Pentabromo AIM 2, MC79 Sc-xrd displaying a *trans, trans, cis* stereochemistry. (B). The unit cell of 2 is the most complex of the examples in the present study and consists of four slightly different three-dimensional orientations, all of which possess the same A-ring stereochemistry.

The additional application of this method on the 10-Cl AIM precursor had similar results, with the bromination of the compound affording a 1,2,3,4-Br 10-Cl analogue with the same stereochemistry as the pentabromo analogue, once again verified using Sc-xrd (Figure 10). Similarly in this case the atropisomers were also found in a 1:1 ratio. The following can be found in Supplementary Materials for tetra bromo chloro AIM 3 (MC221): Figure S8. Numbering for the unit cell, Table S8. Fractional Atomic Coordinates ( $\times 10^4$ ) and Equivalent Isotropic Displacement Parameters ( $\text{\AA}^2 \times 10^3$ ), Table S9. Anisotropic Displacement Parameters ( $\text{\AA}^2 \times 10^3$ ), Table S10. Bond Lengths, Table S11. Bond Angles, Table S12. Torsion Angles, Table S13. Hydrogen Atom Coordinates ( $\text{\AA} \times 10^4$ ) and Isotropic Displacement Parameters ( $\text{\AA}^2 \times 10^3$ ) and Table S14. Atomic Occupancy.



**Figure 10.** Asymmetric unit of tetrabromo chloro AIM 3 Sc-xrd showing the same *trans, trans, cis* stereochemistry. Thermal ellipsoids drawn at the 50% probability level. Disorder not displayed for clarity.

A subsequent base-induced re-aromatization using pyridine [19] afforded a disubstituted 3,10 dibromo anthracenyl isoxazole ethyl ester, which we again verified using Sc-xrd after purification (Figures 11 and 12). The following can be found in Supplementary Materials for dibromo ester 4, (MC219): Figure S9. Numbering; Figure S10. HPLC-MS, Table S15. Atom Coordinates ( $\text{\AA} \times 10^4$ ), Table S16. Anisotropic Displacement Parameters ( $\text{\AA}^2 \times 10^3$ ), Table S17. Bond Lengths, Table S18. Bond Angles, Table S19. Torsions, and Table S20. Hydrogen Atom Coordinates ( $\text{\AA} \times 10^4$ ) and Isotropic Displacement Parameters ( $\text{\AA}^2 \times 10^3$ ). The 3-Br, 10-Cl-compound may provide an opportunity for selective palladation insert at the bromine in the presence of the chloride. The resulting opportunities for metal insertion provides candidates for further development because of the numerous palladium catalyzed methods for substitution (Suzuki, Hartwig, Buchwald, etc., nobelprize.org), which could systematically produce a diversity of AIMs for study from common intermediates.

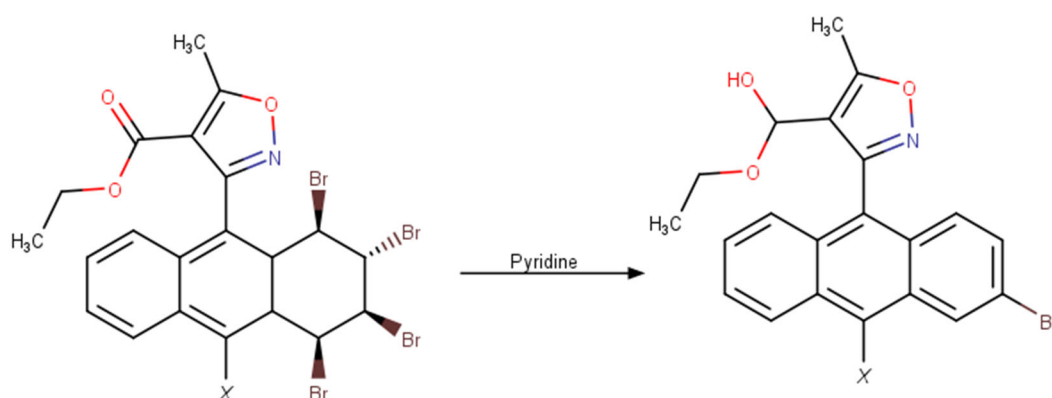


**Figure 11.** Base-induced re-aromatization of the brominated product, where X = Br (92%) or Cl (89%).

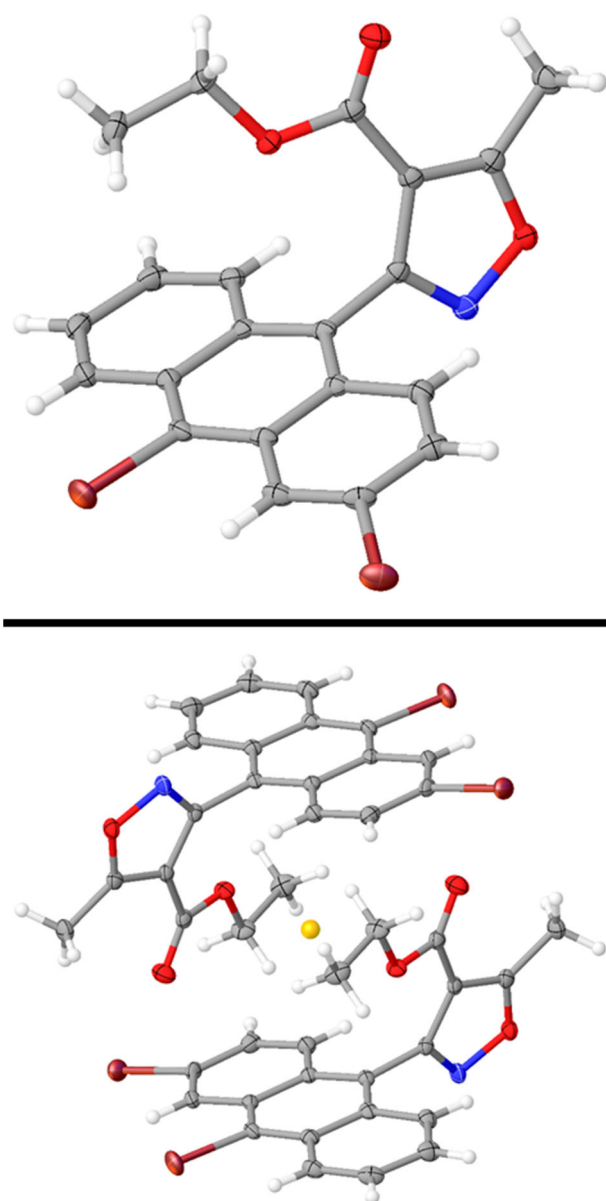


**Figure 12.** Dibromo AIM precursor Sc-xrd (**top**), dibromo AIM precursor Sc-xrd in the unit cell showing a 1:1 M-to-P ratio (**bottom**) at the chiral axis. The yellow dot is an inversion center resulting in the conversion between the two. The thermal ellipsoid plots are drawn at the 50% probability level.

#### 4. Discussion

The stereochemistry observed in the major diastereomeric product from the bromination of these compounds calls for the consideration of the mechanism involved and the influence that the isoxazole ethyl ester has on the resulting stereochemistry. A conventional thought on the addition mechanism of elemental bromine to an aromatic ring by electrophilic aromatic substitution would be the prediction that the resulting stereochemistry would favor a *trans, trans, trans* conformation, minimizing the steric strain on the neighboring bromine atoms. We used the Karplus equation to analyze the J-coupling data observed in the  $H^1$ NMR spectra (Figure 13) in early attempts to decipher the stereochemistry resulting from the bromination of the A-ring. The large coupling constants of 11.23 would seem to suggest a *trans* conformation with respect to the 2 and 3 A-ring protons, also suggesting that the bromines favored an equatorial position, as was noted by Cakmak in his bromination studies. Only after crystallization and an Sc-xrd structural analysis revealing the contortion of the A-ring into a ‘twisted boat’ conformation was it confirmed

that all three angles are rather large, and the major diastereomer is in fact the *trans, trans, cis* conformer previously mentioned.

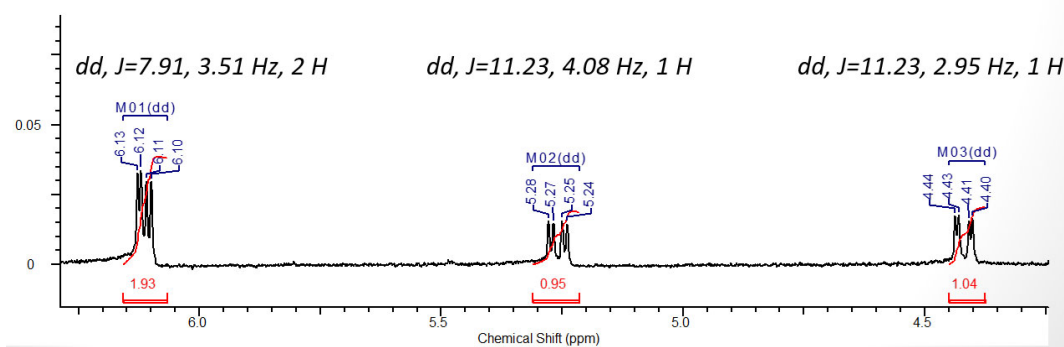


**Figure 13.**  $^1\text{H-NMR}$  of the 1,2,3,4,10-Br analogue **2** zoomed in on the region displaying the J-coupling data associated with the tetra brominated ring, which, when analyzed using the Karplus equation, indicates dihedral angles between hydrogens.

Additionally noteworthy is the fact that while the Cakmak group reported a 45% yield of the major diastereomer (the *trans, trans, cis* isomer), in our efforts on the AIM precursors, the bromination afforded the major diastereomer in 68% (in the case of the 1,2,3,4,10-Br **2**) and 63% (in the case of the 1,2,3,4-Br 10-Cl **3**) of the yields. Cakmak's yields are observed to be less synthetically selective due to the symmetry of their hydrocarbon precursors, where our diastereoselective yields are much closer to the generally accepted, synthetically useful benchmark of 70%. It is reasonable to assume that the isoxazole ethyl ester plays some role in the direction and efficiency of the diastereoselective addition. Although no mechanistic explanation was proposed for the observed stereochemistry in the 2006 Cakmak publication, since we have verified the structure and conformation using Sc-xrd, we believe it is reasonable to propose a  $\text{S}_{\text{N}}2'$  mechanism to explain the observed stereochemistry (Figure 14).

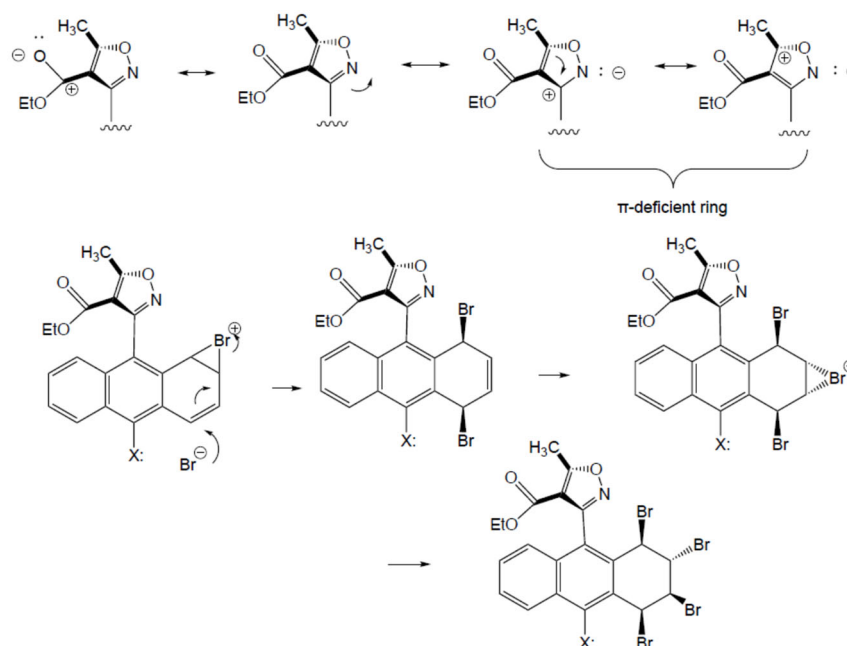


**Figure 14.** The resonance structures of the isoxazole ethyl ester that encourage a stereo-electronic environment that allows for the proposed  $\text{S}_{\text{N}}2'$  mechanism, resulting in the major diastereomer observed in the bromination of the AIM esters **2** and **3**.

We propose that the stereo-electronic environment (Figure 14) produced by isoxazole ethyl ester directs the bromination in a more efficient manner that produces a diastereomeric selective process. In our proposed mechanism, the first bromine addition takes place in the 1-position of the A-ring, forming a 3-membered bromonium ion ring stabilized by the interaction with the  $\pi$ -deficient isoxazole ring. Next, a bromide addition in the 4-position of the A-ring relieves the ring strain of the bromonium, resulting in a 1,4-substitution pattern. This addition across the ring on the same face of the ring seems to be supported by the existence of a crystal structure published in 1985 of a  $\text{Br}_3^-$  ion reported to be interacting with a 3-membered bromonium ring; this  $\text{Br}_3^-$  ion could plausibly span the distance to the 4-position of the A-ring [35]. The 1,4-substitution pattern of the A-ring then likely forces the ring into a chair-like conformation, leaving the remaining double bond on the A-ring open to bromination by the excess bromine in the solution. Proceeding from this point, it is reasonable to assume the next bromide addition forms another bromonium ion by a backside whose ring strain is relieved by the addition of a final bromide ion. The reproducibility of the diastereomeric selectivity in this reaction in both the 10-Cl and 10-Br analogues of the AIM precursors in similar yields supports the hypothesized isoxazole directed mechanism.

## 5. Conclusions

The successful and reproducible diastereoselective bromination and re-aromatization of anthracenyl isoxazole ethyl esters has opened the door to the systematic production of synthetically divergent and accessible AIM precursors. By expanding the selective bromination methodology to the 10-Cl analogues, we have introduced another point of diversification that should enable numerous potential substitutions, including selective palladation insertion at the bromine in the presence of chloride.

With this new synthetic methodology, novel and diverse libraries of compounds can be developed to further define the structure–activity relationship of the potent antitumor series of small molecules known as the AIMs. Additionally, the development of this next generation of asymmetric AIM precursors allows for the investigation of the effect of atropisomerism on the selectivity and activity of the AIMs. A substitution that leads to a sufficient energetic barrier to rotation about the isoxazole-anthryl axis could produce isolable enantiomers that possess a eudismic ratio. Lastly, the attainment of Sc-xrd data on these brominated compounds could lead to a better understanding of the effect of the stereo-electronic environment on the bromination of aromatic hydrocarbons, which could have a significant impact on the field of medicinal chemistry and beyond.

**Supplementary Materials:** The following supporting information can be downloaded at: <https://www.mdpi.com/article/10.3390/cryst14030256/s1>, Figure S1. Proton NMR of the A ring region of the nitrile oxide tetra bromide **6**; Figure S2. Larger version of Figure 5, Structure of Bromo nitrile oxide **1**. (MC59); Figure S3. Larger version of Figure 6. Unit cell for the Bromo nitrile oxide **1** (MC59); Figure S4. Larger version of Figure 7, Halogen Bond for Bromo nitrile oxide **1** (MC59), with a distance of 3.057 Å; Table S1. Fractional atomic coordinates and isotropic or equivalent isotropic displacement parameters ( $\text{\AA}^2$ ) for Bromo Nitrile Oxide **1**, MC59; Table S2. Atomic displacement parameters ( $\text{\AA}^2$ ) for Bromo Nitrile Oxide **1**, MC-59; Table S3. Geometric parameters ( $\text{\AA}$ ,  $^\circ$ ) for (mc59) for Bromo Nitrile Oxide **1**, MC-59; Figure S5. Proton NMR of penta bromo AIM ester **2** (MC79); Figure S6.  $^{13}\text{C}$  NMR of penta bromo ester **2** (MC79); Figure S7. Numbering of unit cell of penta bromo ester **2** (cl\_mc79c9\_15\_0m); Table S4. Fractional atomic coordinates and isotropic or equivalent isotropic displacement parameters ( $\text{\AA}^2$ ) for the Penta bromo AIM ester **2** (cl\_mc79c9\_15\_0m); Table S5. Atomic displacement parameters ( $\text{\AA}^2$ ) for the Penta bromo AIM ester **2** (cl\_mc79c9\_15\_0m); Table S6. Geometric parameters ( $\text{\AA}$ ,  $^\circ$ ) for the Penta bromo AIM ester **2** (cl\_mc79c9\_15\_0m); Table S7. Hydrogen-bond geometry ( $\text{\AA}$ ,  $^\circ$ ) for the Penta bromo AIM ester **2** (cl\_mc79c9\_15\_0m); Figure S8. Numbering for the unit cell for tetra bromo chloro AIM **3** (MC221); Table S8. Fractional Atomic Coordinates ( $\times 10^4$ ) and Equivalent Isotropic Displacement Parameters ( $\text{\AA}^2 \times 10^3$ ) for the tetrabromo Chloro AIM ester **3** (MC221); Table S9. Anisotropic Displacement Parameters ( $\text{\AA}^2 \times 10^3$ ) for the Tetrabromo Chloro AIM ester **3** (MC221); Table S10. Bond Lengths for the Tetrabromo Chloro AIM ester **3** (MC221);

Table S11. Bond Angles for the Tetrabromo Chloro AIM ester **3** (MC221); Table S12. Torsion Angles for the Tetrabromo Chloro AIM ester **3** (MC221); Table S13. Hydrogen Atom Coordinates ( $\text{\AA} \times 10^4$ ) and Isotropic Displacement Parameters ( $\text{\AA}^2 \times 10^3$ ) for the Tetrabromo Chloro AIM ester **3** (MC221); Table S14. Atomic Occupancy for the Tetrabromo Chloro AIM ester **3** (MC221); Figure S9. Numbering for dibromo ester **4** (MC219), umt-nn3; Table S15. Atom Coordinates ( $\text{\AA} \times 10^4$ ) for dibromo ester **4** (MC219), umt-nn3; Table S16. Anisotropic Displacement Parameters ( $\text{\AA}^2 \times 10^3$ ) for dibromo ester **4**, (MC219), umt-nn3; Table S17. Bond Lengths for dibromo ester **4**, (MC219), umt-nn3; Table S18. Bond Angles for dibromo ester **4**, (MC219), umt-nn3; Table S19. Torsions for dibromo ester **4**, (MC219), umt-nn3; Table S20. Hydrogen Atom Coordinates ( $\text{\AA} \times 10^4$ ) and Isotropic Displacement Parameters ( $\text{\AA}^2 \times 10^3$ ) for dibromo ester **4**, (MC219), umt-nn3; Figure S10. HPLC-MS for dibromo ester **4**. Reference [20] is cited in the supplementary materials.

**Author Contributions:** Conceptualization, M.J.C., M.J.W. and N.R.N.; methodology, M.J.C., D.A.D., C.L. and M.J.W.; software, all authors; validation, M.J.C., D.A.D., C.L. and M.J.W.; formal analysis, all authors.; investigation, all authors; resources, D.A.D., C.L. and N.R.N.; data curation M.J.C., D.A.D. and C.L.; writing—original draft preparation, M.J.C., D.A.D., C.L. and N.R.N.; writing—review and editing, D.A.D., C.L. and N.R.N.; visualization, all authors; supervision, N.R.N.; project administration, N.R.N.; funding acquisition, M.J.C., D.A.D. and N.R.N. All authors have read and agreed to the published version of the manuscript.

**Funding:** We thank the National Science Foundation (NSF)-MRI (CHE—1337908) for the funds to obtain the diffractometer, and D.A.D. and M.J.C. thank the National Institute of Health (P30GM140963) for their support and a core fellowship, respectively.

**Data Availability Statement:** The raw data supporting the conclusions of this article will be made available by the authors on request.

**Acknowledgments:** N.R.N. thanks the ALSAM Foundation for a Skaggs Scholar award, which allowed for the collaboration with Donald S. Backos and Philip Reigan at the Anschutz medical campus, where the G4 computation was conducted.

**Conflicts of Interest:** The authors declare no conflicts of interest.

## References

1. Neidle, S. *Quadruplex Nucleic Acids as Targets for Medicinal Chemistry*; Annual Reports in Medicinal Chemistry; Elsevier: Amsterdam, The Netherlands, 2020; Volume 54.
2. Balasubramanian, S.; Hurley, L.H.; Neidle, S. Targeting G-quadruplexes in gene promoters: A novel anticancer strategy? *Nature* **2011**, *10*, 261. [[CrossRef](#)]
3. Neidle, S. *Therapeutic Applications of Quadruplex Nucleic Acids*; Academic Press: Cambridge, MA, USA, 2012.
4. Dervan, P.B. Molecular Recognition of DNA by Small Molecules. *Bioorg. Med. Chem.* **2001**, *9*, 2215–2235. [[CrossRef](#)]
5. Verner, E.J.; Oliver, B.J.; Schlicksupp, L.; Natale, N.R. The Use of Phosphonitric Dichloride Cyclic Trimer in Oligopeptide Synthesis. Synthesis of Isoxazolyl-Prodrugs of Netropsin and Distamycin. *Heterocycles* **1990**, *31*, 327–339. [[CrossRef](#)]
6. Weaver, M.J.; Stump, S.; Campbell, M.J.; Backos, D.S.; Li, C.; Reigan, P.; Adams, E.; Beall, H.D.; Natale, N.R. 10-N-Heterocyclic Aryl-Isoxazole-amides (AIMs) have robust anti-tumor activity against breast and brain cancer cell lines and useful fluorescence properties. *Bioorg. Med. Chem.* **2020**, *28*, 115781. [[CrossRef](#)]
7. Duncan, N.S.; Rider, K.C.; Backos, D.S.; Li, C.; Reigan, P.; Stump, S.; Gajewski, M.P.; Beall, H.D.; Natale, N.R. 10-Alkoxy-anthracenyl-isoxazole analogs have sub-micromolar activity against Glioblastoma multiforme. *Bioorg. Med. Chem.* **2022**, *69*, 116911. [[CrossRef](#)]
8. Toenjes, S.T.; Gustafson, J.L. Atropisomerism in medicinal chemistry: Challenges and opportunities. *Future Med. Chem.* **2018**, *10*, 409–422. [[CrossRef](#)]
9. Dai, J.; Carver, M.; Hurley, L.H.; Yang, D. Solution Structure of a 2:1 Quindoline-c-MYC G-Quadruplex: Insights into G-Quadruplex-Interactive Small Molecule Drug Design. *J. Am. Chem. Soc.* **2011**, *133*, 17673–17680. [[CrossRef](#)]
10. Sevrioukova, I.F.; Poulos, T.L. Structure and mechanism of the complex between cytochrome P450A4 and ritonavir. *Proc. Natl. Acad. Sci. USA* **2010**, *107*, 18422–18427. [[CrossRef](#)]
11. Rider, K.; Burkhart, D.; Li, C.; McKenzie, A.R.; Nelson, J.K.; Natale, N.R. Preparation of chiral isoxazole carbinols via catalytic asymmetric Corey-Bakshi-Shibata reduction. *Arkivoc* **2010**, *viii*, 97–107. [[CrossRef](#)]
12. Rydberg, P.; Gloriam, D.E.; Zaretski, J.; Breneman, C.; Olsen, L. SMARTCyp: A 2D Method for Prediction of Cytochrome P450-Mediated Drug Metabolism. *Med. Chem. Lett.* **2010**, *1*, 96–100. [[CrossRef](#)]
13. Zanger, U.M.; Schwab, M. Cytochrome P450 enzymes in drug metabolism: Regulation of gene expression, enzyme activities, and impact of genetic variation. *Pharmacol. Ther.* **2013**, *138*, 103–141. [[CrossRef](#)]

14. Martin, P.; Oliver, S.; Kennedy, S.J.; Partridge, E.; Hutchison, M.; Clarke, D.; Giles, P. Pharmacokinetics of vandetanib: Three phase I studies in healthy subjects. *Clin. Ther.* **2012**, *34*, 221–237. [[CrossRef](#)]
15. Watson, D.A.; Su, M.; Teverovskiy, G.; Zhang, Y.; García-Fortanet, J.; Kinzel, T.; Buchwald, S.L. Formation of ArF from LPdAr(F): Catalytic Conversion of Aryl Triflates to Aryl Fluorides. *Science* **2009**, *325*, 1661–1664. [[CrossRef](#)]
16. Liang, T.; Neumann, C.; Ritter, T. Introduction of Fluorine and Fluorine-Containing Functional Groups. *Angew. Chem. Int. Ed.* **2013**, *52*, 8214–8264. [[CrossRef](#)]
17. Han, X.; Twamley, B.; Natale, N.R. Preparation of 3-(10'-Halo-9'-anthracenyl)-5-methyl isoxazolecarboxylic Esters. *J. Heterocycl. Chem.* **2003**, *40*, 539–545. [[CrossRef](#)]
18. Mirzaei, Y.R.; Weaver, M.J.; Steiger, S.A.; Kearns, A.K.; Gajewski, M.P.; Rider, K.C.; Beall, H.D.; Natale, N.R. Improved synthesis of 3-aryl isoxazoles containing fused aromatic rings. *Tetrahedron* **2012**, *68*, 10360–10364. [[CrossRef](#)]
19. Cakmak, O.; Aydogan, L.; Berkil, K.; Gulcin, I.; Buyukgungor, O. Highly brominated anthracenes as precursors for the convenient synthesis of 2,9,10-trisubstituted anthracene derivatives. *Beilstein J. Org. Chem.* **2008**, *4*, 50. [[CrossRef](#)]
20. Cakmak, O.; Erenler, R.; Tutar, A.; Celik, N. Synthesis of New Anthracene Derivatives. *J. Org. Chem.* **2006**, *71*, 1795–1801. [[CrossRef](#)]
21. Bruker. APEX2; Bruker AXS Inc.: Madison, WI, USA, 2012.
22. Bruker. SAINT; Bruker AXS Inc.: Madison, WI, USA, 2016.
23. Sheldrick, G.M. SHELXT—Integrated space-group and crystal-structure determination. *Acta Cryst.* **2015**, *A71*, 3–8. [[CrossRef](#)]
24. Sheldrick, G.M. Crystal structure refinement with SHELXL. *Acta Cryst.* **2015**, *C71*, 3–8.
25. Dolomanov, O.V.; Bourhis, L.J.; Gildea, R.J.; Howard, J.A.K.; Puschmann, H. OLEX2: A complete structure solution, refinement and analysis program. *J. Appl. Cryst.* **2009**, *42*, 339–341. [[CrossRef](#)]
26. Sheldrick, G.M. SADABS: Area Detector Absorption Correction; University of Göttingen: Göttingen, Germany, 2001.
27. Bruker. APEX3; Bruker AXS Inc.: Madison, WI, USA, 2016.
28. Sheldrick, G.M. A short history of SHELX. *Acta Cryst.* **2008**, *A64*, 112–122. [[CrossRef](#)] [[PubMed](#)]
29. Grundmann, C.; Dean, J.M. Nitrile Oxides. V. Stable Aromatic Nitrile Oxides. *J. Org. Chem.* **1965**, *30*, 2809–2812. [[CrossRef](#)]
30. Bode, J.W.; Hachisu, Y.; Matsuura, T.; Suzuki, K. Facile construction and divergent transformation of polycyclic isoxazoles: Direct access to polyketide architectures. *Org. Lett.* **2003**, *5*, 391–394. [[PubMed](#)]
31. Bode, J.W.; Hachisu, Y.; Matsuura, T.; Suzuki, K. Amine-promoted cyclocondensation of highly substituted aromatic nitrile oxides with diketones. *Tetrahedron Lett.* **2003**, *44*, 3555–3558. [[CrossRef](#)]
32. Groundwater, P.W.; Nyerges, M.; Fejes, I.; Hibbs, D.E.; Bendell, D.; Anderson, R.J.; McKillop, A.; Sharif, T.; Zhang, W. Preparation and reactivity of some stable nitrile oxides and Nitrones. *Arkivoc* **2000**, *v*, 684–697. [[CrossRef](#)]
33. Dhami, J.K.; Idzorek, K.M.; Johnson, R.B.; Van Auken, K.S.; Ojala, W.H. Intramolecular geometry and intermolecular interactions of the CNO group of crystalline benzonitrile oxides: A comparison with phenyl cyanates, phenyl isocyanates, and phenyl azides. *CrystEngComm* **2019**, *21*, 908–916. [[CrossRef](#)]
34. Donald, K.J.; Pham, N.; Ravichandran, P. Sigma Hole Potentials as Tools: Quantifying and Partitioning Substituent Effects. *J. Phys. Chem. A* **2023**, *127*, 10147–10158. [[CrossRef](#)]
35. Slebocka-Tilk, H.; Ball, R.G.; Brown, R.S. The question of reversible formation of bromonium ions during the course of electrophilic bromination of olefins. 2. The crystal and molecular structure of the bromonium ion of adamantlylideneadamantane. *J. Am. Chem. Soc.* **1985**, *107*, 4504–4508. [[CrossRef](#)]

**Disclaimer/Publisher's Note:** The statements, opinions and data contained in all publications are solely those of the individual author(s) and contributor(s) and not of MDPI and/or the editor(s). MDPI and/or the editor(s) disclaim responsibility for any injury to people or property resulting from any ideas, methods, instructions or products referred to in the content.